



Microstructure and mechanical properties of underwater hyperbaric FCA-welded duplex stainless steel joints

Yu Hu^{a,b}, Yonghua Shi^{a,b,*}, Kun Sun^{a,b}, Xiaoqin Shen^{a,b}, Zhongmin Wang^c

^a School of Mechanical and Automotive Engineering, South China University of Technology, Guangzhou 510640, China

^b Guangdong Provincial Engineering Research Center for Special Welding Technology and Equipment, Guangzhou 510640, China

^c Guangxi Key Laboratory of Information Materials, Guilin University of Electronic Technology, Guilin 541004, China

ARTICLE INFO

Keywords:

Mechanical properties
Duplex stainless steel
Flux-cored arc welding
Underwater welding
TEM
EBSD

ABSTRACT

The microstructure and mechanical properties of underwater hyperbaric flux-cored arc (FCA) welded duplex stainless steel joints were investigated. Ferrite in the heat-affected zone (HAZ) and weld metal (WM) exhibited the same primary micro-texture as the base metal (BM). Austenite in the different zones exhibited different micro-textural components. The low-energy $\Sigma 3$ austenite grain boundaries in the BM were almost two times greater in number than those in the HAZ and WM. Abundant ferrite along with Cr_2N precipitation in the HAZ increased the dislocation density and microhardness of the HAZ, but was detrimental to the elongation of the joint. A balanced ferrite-austenite microstructure in the WM inhibited Cr_2N precipitation. The strength and microhardness of the WM were the highest, with a good elongation of more than 30%. The absorbed energies of the BM and WM at -40°C met the ASTM A923 requirements. This welding process can be used for the maintenance of the spent fuel storage pools.

1. Introduction

Lean duplex stainless steel (LDSS¹) is often considered as an alternative to austenite stainless steel; in LDSS, Ni is substituted by Mn and N. Compared to the corresponding austenite stainless steels, LDSS grades are cheaper due to the lower Ni content. Further, the equal contents of ferrite and austenite in the microstructure of LDSS confer higher strength; at the same time, they do not adversely affect the corrosion resistance of the steel. 2101 LDSS is a relatively new LDSS with a general performance reported to be better than that of AISI 304 or even equal to that of AISI 316 L (AISI refers to austenitic stainless steels). In recent years, LDSS 2101 has been used in the construction of spent fuel storage pools in nuclear power plants. The breakage of these spent fuel storage pools is a potentially serious risk in nuclear power plant operation. In such cases, welding is often used for their maintenance and repair.

In General, 2101 LDSS has good weldability and can be automatically welded. Cui et al. (2018) reported that, 10.8 mm thick 2101 LDSS plates can be well butt jointed by keyhole deep penetration tungsten inert gas welding, without groove and filler metal (FM²). High

contents of Mn and N in 2101 LDSS accelerate austenite transformation in the weld metal (WM³) and the heat-affected zone (HAZ⁴) during welding. However, Westin (2010) found that, filler metal with higher Ni content and shielding gas containing nitrogen are usually used to further improve the austenite content and ensure good resultant mechanical properties and corrosion resistance. Most of the previous studies on 2101 LDSS welds focused on the local corrosion resistance. Hu et al. (2017) studied the evolution of the microstructure and pitting corrosion resistance of multi-pass 2101 LDSS welded joints. Westin and Fellman (2010) found that, CO_2 laser welding and CO_2 laser hybrid welding with gas metal arc are demonstrated to be beneficial to the austenite formation and resultant high critical pitting temperature (CPT) of all the 24 laser welds. Sun et al. (2018) studied the intergranular corrosion resistance of underwater dry and wet 2101 LDSS welds. However, literature on the mechanical properties of 2101 LDSS welded joints is scarce. It should be realized that owing to the increasing use of 2101 LDSS as a structural material, the mechanical properties of 2101 LDSS joints should be paid more attention.

Zhang et al. (2006) pointed out that underwater welding is often employed for maintenance and repair in offshore engineering. So far,

* Corresponding author at: School of Mechanical and Automotive Engineering, South China University of Technology, Guangzhou 510640, China.

E-mail address: yhuashi@scut.edu.cn (Y. Shi).

¹ Lean duplex stainless steel.

² Filler metal.

³ Weld metal.

⁴ Heat affected zone.

almost all the reports on underwater welding of duplex stainless steel (DSS⁵) focused on standard DSS. Akselsen et al. (2009) investigated the weldability, microstructure, and resultant properties of 2205 DSS hyperbaric welded at 1.2 MPa and 3.5 MPa. łabanowski et al. (2016) confirmed the good weldability at underwater conditions of 2205 DSS using metal manual arc welding; however, the difficulties in stable arc burning were also revealed. However, with the increasing application of LDSS in offshore engineering, it is necessary to study the underwater welding technology of LDSS. Shi et al. (2013) were the first to investigate the effect of water depth on the bead geometry of underwater wet-welded lean 2101 welds. However, Shi et al. (2017) indicated that the existence of porosity impeded further studies on the properties of 2101 underwater wet-welded joints. Guo et al. (2017) also suggested the existence of welding defects, such as porosity and bad weld morphology, during wet welding. Jia et al. (2013) detected the peak of H atom in the spectrum signal of underwater wet welding, and revealed that the presence of H element makes the underwater environment complex and significantly influences the underwater wet welding stability. Thus, considering that a good weld quality is needed for practical offshore engineering, studies on dry underwater welding of LDSS are very important and meaningful.

The purpose of the present investigation is to study underwater hyperbaric welding technology and evaluate the microstructural evolution and mechanical properties of 2101 LDSS joints welded using the flux-cored arc (FCA⁶) welding technology in a hyperbaric chamber.

2. Experimental

2.1. Materials and welding process

The base metal (BM⁷) UNS S32101 was hot-rolled to a thickness of 10 mm, solution-annealed at 1030 °C, and quenched. 2101 LDSS plates with dimensions of 300 × 100 × 10 mm³ were assembled into the shape of a V-groove with a groove angle of 40° and root opening of 2 mm, as shown in Fig. 1(a). The FM used was an ER 2209 flux-cored wire with a diameter of 1.2 mm. The chemical composition of the BM and FM are listed in Table 1, and the optimized welding parameters are listed in Table 2. Before welding in the hyperbaric chamber, the authors referred to previous reports related to DSS FCA butt welding parameters in air, according to Kang and Lee (2012). Then, the authors attempted to correct the welding current, welding voltage and welding speed to perform the welding experiment in the hyperbaric chamber. The experimental setup of underwater welding consists of a high-pressure underwater welding simulation chamber, a welding power source, a three-dimensional motion platform, and other auxiliary equipment. Before welding, compressed air was pressurized into the chamber to simulate water pressure, which increased with increasing water depth. This investigation was conducted at a pressure of 0.45 MPa, which is equivalent to a water depth of 45 m. The pressure inside the chamber could be read through a pressure gauge installed on the chamber. Before welding, the pressure inside the chamber was adjusted to 0.45 MPa. During welding, the pressure inside the chamber was verified manually. The gas outlet was opened when the pressure was higher than 0.45 MPa. Generally, the welding time of each weld pass was too short to cause a change in the pressure inside the chamber greater than 0.02 MPa.

2.2. Microstructural characterization

The microstructure of the welded joints in the transverse direction (TD⁸) was revealed using a Beraha II solution (1 g K₂S₂O₅ + 30 mL HCl

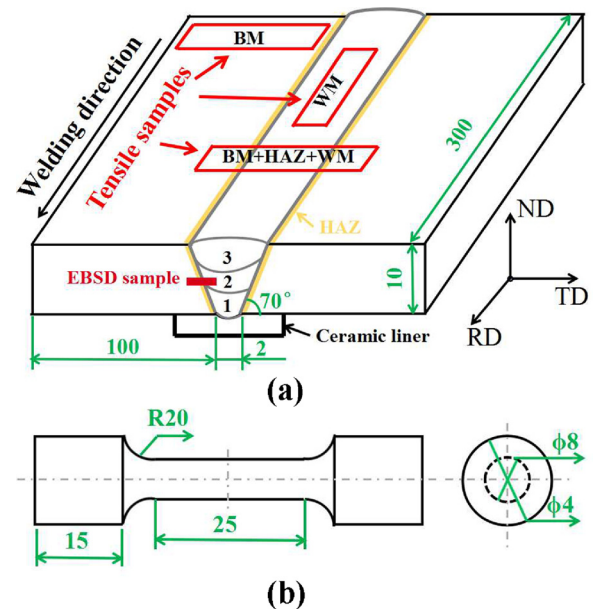


Fig. 1. Schematic illustrations of the welded joint and the tested samples. (a) The welded joint, the location of tensile and EBSD samples (red rectangle) and (b) the size of the tensile samples. All units are in mm (For interpretation of the references to colour in this figure legend, the reader is referred to the web version of this article).

+ 60 mL H₂O). The microstructures were then characterized using optical microscopy (OM⁹), scanning electron microscopy (SEM¹⁰), and transmission electron microscopy (TEM¹¹). The austenite content was calculated automatically via the image analysis software Image-Pro Plus. The orientation information, grain boundaries, and local misorientations of the DSS joint were evaluated by electron backscatter diffraction (EBSD¹²) analysis, which was conducted in the TD - rolling direction (RD¹³) plane. The normal direction (ND¹⁴) was vertical to the TD–RD plane, as shown in Fig. 1(a). The OM, SEM, and TEM images were captured along the TD–ND plane.

2.3. Mechanical behavior and microhardness testing

Sub-size tensile test specimens of the welded joints were prepared along the transverse or rolling direction, as shown in Fig. 1(a). The tensile tests were conducted on a universal testing machine, at a loading rate of 3 mm/min. A schematic of the tensile sample is shown in Fig. 1(b). Charpy V-notch (CVN¹⁵) impact tests were conducted at –40 °C. Standard sub-size CVN samples (55 × 10 × 7.5) mm³ were machined along the TD according to the ASTM A370 (2015). The center lines of the tensile and CVN samples coincided with those of the weldment. Each test was repeated three times. The micro-hardness test was carried out using a Vickers hardness tester with 500 g loading and a dwell time of 10 s.

3. Results

3.1. Microstructural characterization

Fig. 2 shows the microstructures and austenite contents ($\gamma\%$) in the

⁵ Duplex stainless steel.

⁶ Flux-cored arc.

⁷ Base metal.

⁸ Transverse direction.

⁹ Optical microscopy.

¹⁰ Scanning electron microscopy.

¹¹ Transmission electron microscopy.

¹² Electron backscatter diffraction.

¹³ Rolling direction.

¹⁴ Normal direction.

¹⁵ Charpy V-notch.

Download English Version:

<https://daneshyari.com/en/article/7176232>

Download Persian Version:

<https://daneshyari.com/article/7176232>

[Daneshyari.com](https://daneshyari.com)